Stability of Helicopters in Compliant Contact Under PD-PID Control

Paul E. I. Pounds, *Member, IEEE*, and Aaron M. Dollar, *Senior Member, IEEE*

***Abstract*—Aerial vehicles are difficult to stabilize, especially when acted upon by external forces. A hovering vehicle interacting with objects and surfaces must be robust to contact forces and torques transmitted to the airframe. These produce coupled dynamics that are distinctly different from those of free flight. While external contact is generally avoided, extending aerial robot functionality to include contact with the environment during flight opens up new and useful areas such as perching, object grasping, and manipulation. These mechanics may be modeled as elastic couplings between the aircraft and the ground, represented by springs in $\mathbb{R}^3 \times$SO(3). We show that proportional derivative and proportional integral derivative (PID) attitude and position controllers that stabilize a rotorcraft in free flight will also stabilize the aircraft during contact for a range of contact displacements and stiffnesses. Simulation of the coupled aircraft dynamics demonstrates stable and unstable modes of the system. We find analytical measures that predict the stability of these systems and consider, in particular, the planar system in which the contact point is directly beneath the rotor. We show through explicit solution of the linearized system that the planar dynamics of the object–helicopter system in vertical, horizontal, and pitch motion around equilibrium remain stable, within a range of contact stiffnesses, under unmodified PID attitude control. Flight experiments with a small-scale PID-stabilized helicopter fitted with a compliant gripper for capturing objects affirm our model's stability predictions.**

***Index Terms*—Aerial manipulation, mobile manipulation, unmanned aerial vehicles (UAVs).**

I. Introduction

UNMANNED aerial vehicles (UAVs) have demonstrated their ability to fly, maneuver, and carry out observation tasks. There is growing interest in using UAVs to interact with their environments. The ability to manipulate objects while hovering will allow these vehicles to be used for infrastructure maintenance and other similar tasks in locations that are inaccessible to terrestrial vehicles, such as the tops of power lines and radio masts, rough terrain, or water surfaces.

When an aircraft contacts a surface, forces are transmitted to the airframe that may destabilize the vehicle if not properly accounted for. Such perturbations arise both when actively engaging and manipulating objects, as well as during inadvertent collisions. Continued stability when subject to these forces is essential for safe operation.

A. Previous Work

Aircraft–object interactions have historically been in the form of tethered flight and surface contact in landing, with care taken to avoid pathological coupled modes, such as dynamic rollover [14]. Work on UAV–object interaction has followed these lines of inquiry. The dynamics of an aircraft tethered to ground are important for landing helicopters on ships.[1] Research into tethered unmanned helicopter stability has been conducted since the 1960s. An early paper describes two fundamental flight modes of tethered helicopters [5]: stability of attitude due to the low connection point of the tether, and pure instability in position, the so-called pendulum mode. These dynamics have been exploited to produce a stable unmanned rotor platform that flew at the end of its tether in a local equilibrium where the tether tension, weight, and rotor thrust were balanced by automatic control [6]. More recently, efforts have focused on autonomous landing of helicopters on ships in rough weather using a tether winch [7], [8].

All of these papers consider the helicopter to be flying far from the tether point, where the line tension and direction is approximately constant. However, this is not germane to object interactions in which forces change dynamically. The applied load cannot be treated as a constant either in magnitude or direction, nor always in tension; consequently, the mechanics are quite distinct from previous models. A different analytical approach must be taken, which specifically includes the unique dynamics loadings transmitted to the airframe through the end-effector.

In addition to ground contact, researchers at Università di Bologna (Bologna, Italy) have explored the interaction of a ducted-fan UAV with hard point-contacts flying against sloped and vertical surfaces [1]. Gentili *et al.* employ a state-machine-based mode switching controller that dynamically changes its flight control law as the aircraft transitions from one distinct contact configuration to another. This work was extended to a quadrotor model with a similar control strategy [3], [15]. Researchers at University of Pennsylvania (Philadelphia, PA,

[1] This should not be confused with the dynamics of a helicopter carrying a slung load. When the load rests on the ground, a slung load behaves like a ground tether, but in flight, the load–helicopter system is a two-body dynamic problem and quite different from compliant ground contact [12], [13].

Manuscript received February 25, 2012; revised May 18, 2014; accepted October 7, 2014. Date of current version December 3, 2014. This paper was recommended for publication by Associate Editor T. Hamel and Editor G. Oriolo upon evaluation of the reviewers' comments. This work was supported in part by the Office of Naval Research under Grant N000141010737. Portions of this paper were presented at the Dynamic Systems and Control Conference, 2010 [16], International Conference on Robotics and Automation 2011 [17], and Intelligent Robots and Systems Conference 2011 [18].

P. E. I. Pounds is with the School of Information Technology and Electrical Engineering, University of Queensland, Brisbane, Qld. 4072, Australia (e-mail: paul.pounds@uq.edu.au).

A. M. Dollar is with the Department of Mechanical Engineering and Materials Science, Yale University, New Haven, CT 06511 USA (e-mail: aaron.dollar@yale.edu).

This paper has supplementary downloadable material available at http://ieeexplore.ieee.org.

Color versions of one or more of the figures in this paper are available online at http://ieeexplore.ieee.org.

Digital Object Identifier 10.1109/TRO.2014.2363371

1552-3098 © 2014 IEEE. Personal use is permitted, but republication/redistribution requires IEEE permission.
See http://www.ieee.org/publications_standards/publications/rights/index.html for more information.

Fig. 1. Yale aerial manipulator platform with compliant ventral gripper.

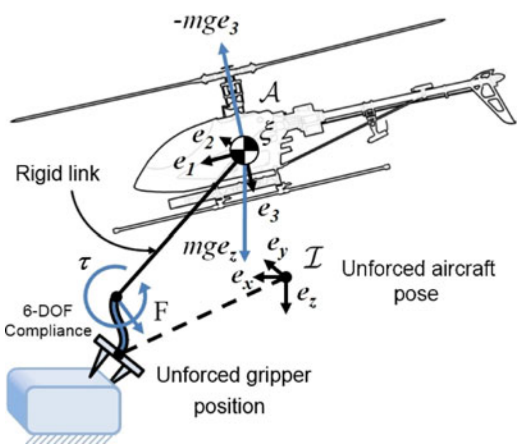

Fig. 2. Aircraft free body diagram.

USA) have exploited high-precision control indoors using Vicon to control contact forces during hover [2], but this is not currently generalizable to outdoor flight due to the sensitivity of Vicon to ambient IR.

B. Contact Compliance Approach

Rather than treat interactions as constant bias or mechanically distinct configurations, our approach is to model contact as serial compliance[2] through an end-effector, probe, or other part of the aircraft [18]. By understanding the behavior of elastically coupled aircraft mechanics under closed-loop flight control, stable configurations of end-effector compliance and displacement from the aircraft center of mass can be identified [16]. This is motivated by the authors' work in utilizing a flexible gripper with both angular and translational stiffness, to grasp and manipulate target objects from a helicopter platform [17]. The compliant-contact framework also applies to cases such as ground contact with landing gear, pushing objects with landing skids, or touching a wall with a rotor shroud.

The authors have developed a test-bed helicopter platform—the Yale Aerial Manipulator—to explore compliant contact of hovering vehicles (see Fig. 1). The aircraft uses a compliant underactuated gripper, based on the SDM Hand [4], which is

[2]Compliance here is taken to mean spring-like behavior where elastic displacement of the end-effector structure is involved (with respect to the vehicle or the ground), as distinct from rigid contact where little relative motion occurs.

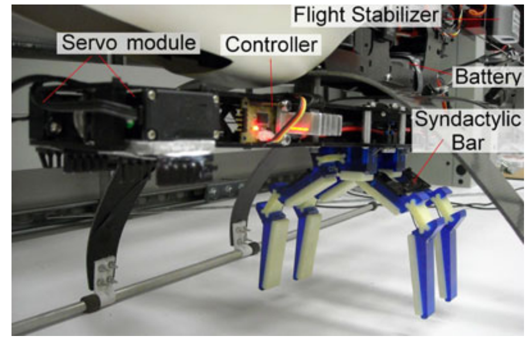

Fig. 3. Test platform mounting compliant gripper module.

mounted ventrally between the skids of a 4.3-kg 1.5-m rotor, T-Rex 600 ESP radio control helicopter (Align, Taiwan). The gripper consists of four fingers with two elastic joints each, actuated by a parallel tendon mechanism that balances loads across each digit. It has a grasp span of 115 mm (see Fig. 3). The helicopter is stabilized in attitude with a Helicommand configured to implement proportional derivative (PD) flight controller (Captron, Germany), directed by a human pilot. The platform can carry loads over 1.5 kg, limited only by the carrying capacity of the helicopter.

The special characteristics of the hand design—open-loop adaptive grasping, wide finger span, insensitivity to positional error [4]—closely match the challenges associated with the UAV manipulation task, allowing for a very simple lightweight mechanism, without the need for imposed structural constraints on the load. To acquire an object, the helicopter approaches the target, descends vertically to hover over the target and then closes its gripper. Once a solid grasp is achieved, the helicopter ascends with the object.

Commercial off-the-shelf flight stabilizers employing PD and proportional integral derivative (PID) architectures are increasingly available for UAV rotorcraft. Rather than employ custom designs tailored for object interactions, it is desirable to use these standard controllers to maintain stability during contact. Many commercial systems are not adjustable mid-flight, and therefore, the same gains that regulate free flight would ideally continue to stabilize the aircraft in contact. By finding compliance limits that guarantee continued stability and designing the contact mechanism appropriately, the controller's free air flight performance can be retained without risk of destabilization in contact. Such tuned stiffnesses ensure stability without knowledge about the contact and are effective even during uncertain contact configurations or unexpected collision.

C. Roadmap

This work expands upon the authors' previous work on coupled flight mechanics, reconciling the results of planar and 6-degrees-of-freedom (DOF) analysis [16], [18]. The more general 6-DOF case is readily applicable to quadrotors, while complex aerodynamics included in the planar case are important for conventional helicopters. Furthermore, this study introduces experimental tests of the stability bounds predicted for end-effector offset configuration.

We begin this paper by producing a 6-DOF stability analysis of rotorcraft mechanics under PD control in $\mathbb{R}^3 \times \mathrm{SO}(3)$. In Section II, we employ a subset of these dynamics for control analysis and present an end-effector compliance model; we describe PD flight controllers employing time-scale separation that stabilize the aircraft in free air. These control laws are used to derive bounds within which the aircraft will remain stable during contact We present simulations of stable and unstable configurations.

We then reduce the complete system to the planar case. A 3-DOF flight model, including vertical rotor damping and ground effect, is presented in Section III, along with a PID controller that stabilizes pitch (but not translation). We examine the specific case of the Yale Aerial Manipulator's gripper mounted ventrally, using a bogie suspension approximation of the SDM hand grasping a fixed object. Coupled pitch-longitudinal translation motion of the helicopter-linkage system is analyzed for stability, and vertical motion of the system is shown to be intrinsically stable.

In Section IV, we test conclusions drawn from the 6-DOF and planar analysis by exploring stability of the aircraft in coupled-flight experiments. We examine an archetypical end-effector configuration with large displacement from the CoG (near the unstable boundary) and show that it is stable given a spring network that closely approximates idealized 6-DOF compliance. We then show experimentally that the standard configuration of the Yale Aerial Manipulator design with a compliant gripper is also stable, both when grasping an object fixed to ground and throughout the partial contact condition when lifting off with the object. Section V concludes this paper.

II. Six-Degrees-of-Freedom Dynamic Model and Contact Stability

The fundamental dynamics of small-scale helicopters are well established [8], [9], [19], [20]. These models typically include the mechanics of a rotating and translating rigid body, driven by a pair of rotors that produce torques and forces at some offset from the center of mass. In this section, we will outline a complete nonlinear model representing complex rotor and vehicle dynamics and, then, employ a simplified 6-DOF version to facilitate control analysis and examine how adding spring forces effect the stability of the system. The planar case of the complete model will be used (see Section III).

A. Free Air Dynamic Model

The inertial reference frame is denoted by $\mathcal{I}=\{\mathbf{e}_x, \mathbf{e}_y, \mathbf{e}_z\}$, where $\mathbf{e}_z$ is in the direction of gravity, and $\boldsymbol{\xi} = (x, y, z)$ is the origin of the body fixed frame $\mathcal{A} = \{\mathbf{e}_1, \mathbf{e}_2, \mathbf{e}_3\}$, where $\mathbf{e}_1$ is aligned with the front of the craft (see Fig. 2). The frame $\mathcal{A}$ is related to $\mathcal{I}$ by the rotation matrix $R : \mathcal{A} \rightarrow \mathcal{I}$. Vector $\mathbf{v}$ is the translational velocity of frame $\mathcal{A}$ in $\mathcal{I}$, and $\boldsymbol{\Omega}$ is angular velocity of frame $\mathcal{A}$ expressed in $\mathcal{A}$.

The system dynamic equations are

$$\dot{\boldsymbol{\xi}} = \mathbf{v} \tag{1}$$

$$m\dot{\mathbf{v}} = mg\mathbf{e}_z + R\mathbf{T}_M + R\mathbf{T}_T \tag{2}$$

$$\dot{R} = R\boldsymbol{\Omega}_\times \tag{3}$$

$$\mathrm{J}\dot{\boldsymbol{\Omega}} = -\boldsymbol{\Omega}_\times \mathrm{J}\boldsymbol{\Omega} + \mathbf{T}_{M\times}\mathbf{h} + \mathbf{T}_{T\times}\mathbf{l} + \boldsymbol{\tau}_M\mathbf{e}_3 + \boldsymbol{\tau}_T\mathbf{e}_2 \tag{4}$$

where m and J are the mass and rotational inertia of the aircraft, respectively; g is the acceleration due to gravity; $\mathbf{T}_M$, $\boldsymbol{\tau}_M$, $\mathbf{T}_T$, and $\boldsymbol{\tau}_T$ are the thrust and drag torque vectors produced by the main rotor and tail rotor, respectively; and $\mathbf{h}$ and $\mathbf{l}$ are their displacements from the center of mass. Here, $\times$ is the skew-symmetric matrix operator.

The rotor of the helicopter is free to "flap" (or pivot) at the center like a see-saw. In horizontal motion, on-coming wind causes an imbalance in lift between the blades on each side of the rotor disc. This causes the rotor plane to pitch upward, changing the angle of attack of each blade until a new equilibrium is reached.

The angled rotor directs some of its thrust aft, slowing the helicopter and producing a pitching moment. Flapping dynamics are an important part of helicopter stability analysis, even at low speeds. The rotor pitch response is extremely fast, and therefore, it can be represented analytically, without need for additional states.

At low speeds, the flapping angle β produced by a zero flapping hinge-offset rotor head is an approximately linear combination of the longitudinal translation and pitch velocities:

$$\beta = q_1\dot{x} - q_2\dot{\theta} \tag{5}$$

where q_1 and q_2 are constant parameters of the rotor [9]. This can be extended to 6-DOF by including the lateral components of flapping and abstracting the distortion of the rotor tip plane to include arbitrary velocities:[3]

$$\mathbf{T}_M = -\alpha_M u_4 \Big(I + [-u_2 u_1 0]'_\times - (Q_1\mathbf{v}_\times\mathbf{e}_3)_\times - (Q_2\boldsymbol{\Omega})_\times\Big)\mathbf{e}_3 \tag{6}$$

$$\mathbf{T}_T = -\alpha_T u_3 \mathbf{e}_2 \tag{7}$$

where I is the 3×3 identity matrix, and α_M and α_T are thrust scaling of the rotors with blade angle of attack. The control inputs u_i are the absolute rotor blade pitch angle controls: u_1 and u_2 are the lateral and longitudinal rotor cyclic pitch, and u_3 and u_4 are the tail rotor and main rotor collective pitch, respectively. Matrices Q_1 and Q_2 are constant translation and rotation flapping parameters of the rotor, respectively:

$$Q_1 = q_1(\mathbf{e}_1 \quad \mathbf{e}_2 \quad 0) \tag{8}$$

$$Q_2 = q_2(\mathbf{e}_1 \quad \mathbf{e}_2 \quad 0) + \frac{1}{\omega_0}(\mathbf{e}_2 \quad \mathbf{e}_1 \quad 0) \tag{9}$$

where q_1 and q_2 are the same rotor translation and rotation parameters used in the planar model [16], and ω_0 is the angular velocity of the rotor.

B. Simplified Analytical Model

The full model above is directly solvable in the planar case but difficult to analyze in 6-DOF. We use a common simplified

[3]This generalizes the model given in [9], which represented rotor flapping as a transformation between body velocity and locally observed rotor wind velocity.

model to yield an easier system to analyze, while retaining its essential behavior; these dynamics are homologous to a quadrotor. The complete model is used for the simulations in Section II-G. Under closed-loop control around equilibrium, the influence of flapping mechanics on system stability is small. Mahony *et al.* note that the lateral forces induced by cyclic controls are small and can be ignored [19]. Rotor inflow damping and ground effect forces are also ignored. However, all these forces are included in our simulations.

The simplified 6-DOF form imparts hierarchal structure to the dynamics, with no feed-forward mechanics is:

$$\dot{\xi} = \mathbf{v} \tag{10}$$

$$m\dot{\mathbf{v}} = mg\mathbf{e}_z - TR\mathbf{e}_3 \tag{11}$$

$$\dot{R} = R\boldsymbol{\Omega}_\times \tag{12}$$

$$\mathbf{J}\dot{\boldsymbol{\Omega}} = -\boldsymbol{\Omega}_\times \mathbf{J}\boldsymbol{\Omega} + \boldsymbol{\Gamma} \tag{13}$$

where $T = mg + \alpha_M \delta u_4$. Control inputs are the sum of trim equilibrium values, plus variation around these points: $u_i = u_{0i} + \delta u_i$. We combine cyclic and tail inputs into a single control vector $\boldsymbol{\Gamma} = [\delta u_2 \quad \delta u_1 \quad \delta u_3]'$.

C. Contact Model

Consider a UAV equipped with an end-effector mounted some displacement $\mathbf{d}$ from its center of mass, in the body-fixed frame. When the end-effector contacts an object or surface, the dynamics of the closed-loop system will change. We represent contact and interaction with objects by a multidimensional elastic coupling; this coupling transmits forces from the aircraft to the object and *vice versa*. We consider the case where the end-effector has a firm grasp and produces stiffness in all axes, but in the future, these models may also be adapted for unidirectional surface contact constraints.

We approximate a compliant end-effect by a multidimensional spring that can apply both angular and translational forces. This model does not consider chatting contact or slip (although these phenomena may have important implications in the stability of system where they are strongly exhibited).

The initial pose of the aircraft is given by $\boldsymbol{\xi}_0$ and R_0. When $\boldsymbol{\xi} = \boldsymbol{\xi}_0$ and $R = R_0$, the end-effector is touching the object with zero force and torque.

Informed by the work of Lončarić [21], we consider a pair of springs: one 3-DOF translational spring and one 3-DOF rotational spring that act on the body to produce a force and geodesic torque (see Fig. 4):

$$\mathbf{F}_\xi = -K_\xi(R\mathbf{d} - R_0\mathbf{d} + \boldsymbol{\xi} - \boldsymbol{\xi}_0) \tag{14}$$

$$\boldsymbol{\tau}_R = -K_R\psi \tag{15}$$

where K_ξ and $K_R = k_R I$ are translational and rotational spring stiffness matrices, respectively, and $\psi_\times = \log(R_0' R)$, where $\log(R)$ is the $\mathfrak{so}(3)$ mapping of the matrix logarithm of $R(\psi)$:

$$\log(R) = \theta\boldsymbol{\omega}_\times \tag{16}$$

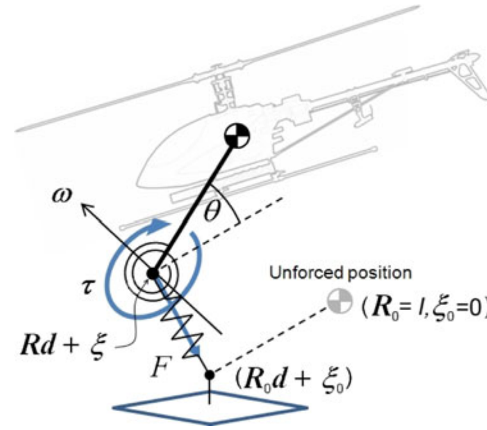

Fig. 4. Contact spring configuration.

where θ and $\boldsymbol{\omega}$ are the angle–axis pair of the exponential representation of the body attitude [22]:

$$\theta = \arccos\left(\frac{\mathrm{trace}(R) - 1}{2}\right) \tag{17}$$

$$\boldsymbol{\omega} = \frac{1}{2\sin(\theta)}\begin{pmatrix} R_{32} - R_{23} \\ R_{13} - R_{31} \\ R_{21} - R_{12} \end{pmatrix}. \tag{18}$$

In this paper, we will only consider the condition where the aircraft starts level at the origin ($\boldsymbol{\xi}_0 = 0$ and $R_0 = I$), but the approach may be extended to consider other starting configurations. The rest pose of the end-effector, $(R_0' R)$ and $(R_0\mathbf{d} + \boldsymbol{\xi}_0)$, will be hereafter simplified to just R and $\mathbf{d}$ in the inertial frame. Note that in the unforced configuration, $R\mathbf{d} + \boldsymbol{\xi} = \mathbf{d}$.

As the end-effector compliance is offset from the aircraft center of mass by $\mathbf{d}$, the forces and torques are coupled. The force induces a moment about the center of mass:

$$\boldsymbol{\tau}_\xi = K_\xi(R\mathbf{d} - \mathbf{d} + \boldsymbol{\xi})_\times \mathbf{d}. \tag{19}$$

Similarly, the rotational spring torque induces forces on the body as

$$\mathbf{F}_R = \frac{k_R \mathbf{d}_\times \psi}{||\mathbf{d}|| ||\boldsymbol{\omega}_\times \mathbf{d}||} \tag{20}$$

which is approximated by $F_R = k_R ||\mathbf{d}||^{-2}\mathbf{d}_\times \psi$.

D. Closed-Loop Free Air Stability

Aircraft flight controllers are designed to stabilize the vehicle in free air. We consider a flight controller employing PD control to stabilize attitude and then position (see Fig. 5).

We make the key assumption that the two sets of dynamics are time-scale separated. Small-scale helicopters typically have pitch and roll dynamics that are an order of magnitude faster than their translational dynamics [16], [20]. In general, however, the interaction between pitch and translation oscillatory modes is nontrivial and to be avoided.[4]

[4]This is specifically considered in Section III.

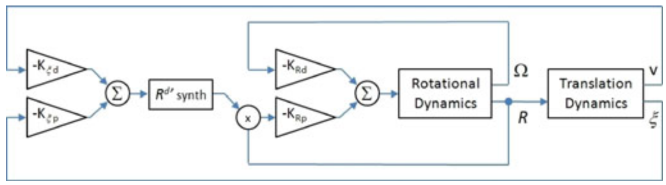

Fig. 5. Flight control architecture.

We apply the analysis by Bullo and Murray for stabilizing a rigid body on SO(3) and $\mathbb{R}^3$ with PD control [22]. They prove stability for second-order systems of this type by constructing Lyapunov energy functions for the angular and translational motions and showing that the derivatives of these functions are negative definite. The attitude dynamics of (13) are exponentially stabilized at $R = I$ by a controller of the form:

$$\mathbf{\Gamma} = -f(R, \mathbf{\Omega}) - K_{Rp}\psi - K_{Rd}\mathbf{\Omega} \tag{21}$$

where $f \in \mathfrak{so}(3)$ is the "internal drift" arising from system coriolis forces $[\mathbf{J\Omega}, \mathbf{\Omega}]$, and K_{Rp} and K_{Rd} are symmetric positive-definite gain matrices, provided

$$\lambda_{\min}(K_{Rp}) > \frac{||\mathbf{\Omega}(0)||^2}{\pi^2 - ||R(0)||^2_{\mathrm{SO}(3)}} \tag{22}$$

where $\lambda_{\min}$ is the smallest eigenvalue of K_{Rp}, $\mathbf{\Omega}(0)$ and $R(0)$ are the initial velocity conditions, and $||R||_{\mathrm{SO}(3)} = \langle \log(R), \log(R)\rangle^{\frac{1}{2}}$ is the ad-invariant metric on SO(3) that gives the arc distance between R and I. This bound is a necessary and sufficient condition for guaranteeing stability under PD [22].

In the case where the proportional gain is $K_{Rp} = k_{Rp}I$, the properties of the skew-symmetric operator and passivity of the coriolis forces allows the controller to be reduced to pure PD form, and the stable system posed in the same structure as (13):

$$\mathbf{J}\dot{\mathbf{\Omega}} = -\mathbf{\Omega}_\times \mathbf{J\Omega} - k_{Rp}\psi - K_{Rd}\mathbf{\Omega}. \tag{23}$$

The $k_{Rp}\psi$ term is a torque proportional to the minimum geodesic distance between the inertial basis frame and the rotated body coordinate frame—conceptualized as the torque generated by such reference frames with springs attached at each basis vector (see Fig. 6).

Assuming time-scale separation between the attitude and translation dynamics, translational mechanics can be treated independently from rotation. Position control is implemented by a trajectory of R and δu_4 that produces desired horizontal and vertical forces. It is straightforward to see that a PD control function will stabilize position

$$m\dot{\mathbf{v}} = -K_{\xi p}\boldsymbol{\xi} - K_{\xi d}\mathbf{v} \tag{24}$$

where $K_{\xi p}$ and $K_{\xi d}$ are the positive-definite gains of a PD control function $\mathbf{U}_\xi$. The orientation of the vehicle is set such that the sum of rotor and gravity forces produces the control function:

$$mg\mathbf{U}_\xi = mg\mathbf{e}_z - TR\mathbf{e}_3. \tag{25}$$

A method for constructing desired orientation R^d that satisfies this equation is given in Appendix A.

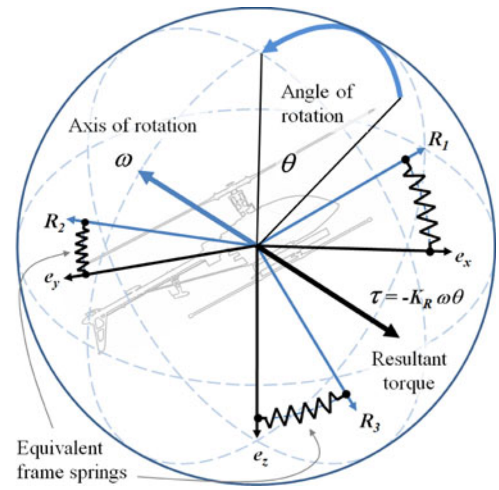

Fig. 6. SO(3) Geodesic Displacement Torque.

E. Stability During Contact

The aircraft velocity dynamics with coupled elastic forces are

$$\begin{aligned} m\dot{\mathbf{v}} = & -K_{\xi p}\boldsymbol{\xi} - K_{\xi d}\mathbf{v} - K_\xi(R\mathbf{d} - \mathbf{d} + \boldsymbol{\xi}) \\ & + k_R||\mathbf{d}||^{-2}\mathbf{d}_\times\psi \end{aligned} \tag{26}$$

$$\begin{aligned} \mathbf{J}\dot{\mathbf{\Omega}} = & -\mathbf{\Omega}_\times\mathbf{J\Omega} - k_{Rp}\psi - K_{Rd}\mathbf{\Omega} \\ & - k_R\psi + K_\xi(R\mathbf{d})_\times\mathbf{d} - \mathbf{d}_\times K_\xi\boldsymbol{\xi}. \end{aligned} \tag{27}$$

The elastic forces can enter the dynamics directly due to the hierarchial structure of the mechanics. It is assumed that $R_0 = I$. Under the assumption of time-scale separation, rotational contributions in the lateral dynamics are ignored, and translational contributions in rotational dynamics are treated as constant.

1) Rotation: Rotational stability requires that (22) remains satisfied for the system without translational disturbance forces and that constant disturbance induced by translational spring force is rejected.

Proportional rotation stiffness and attitude control action are posed in the form of the logarithmic angle-axis displacement of the system; we would like to cast all the rotational compliance terms in the same form. However, the coupled $(R\mathbf{d})_\times\mathbf{d}$ force-lever structure does not support a moment in the direction of $\mathbf{d}$ and, therefore, cannot be exactly expressed as an isotropic logarithmic gain. That said, free-air aircraft rotation in the $\mathbf{d}$ direction is known to be *a priori* stable. We consider, therefore, a more stringent scenario in which rotation in $\mathbf{d}$ is augmented with an additional single-axis torsional spring to produce a combined rotational stiffness in the form $-K_\xi||\mathbf{d}||^2\psi$, which approximates an isotropic 3-DOF torsional spring (see Fig. 7). The positive-definite gain matrices of the proportional torques can then be directly summed.

The eigenvalues of the combined gain will be larger than or equal to those of $k_{Rp}I$ alone. Therefore, the addition of proportional elastic rotational forces will not violate (22) and destabilize the aircraft at I. However, rotational spring forces work to return the rotation of the body to I; to reach R^d to apply the translational control action, the proportional

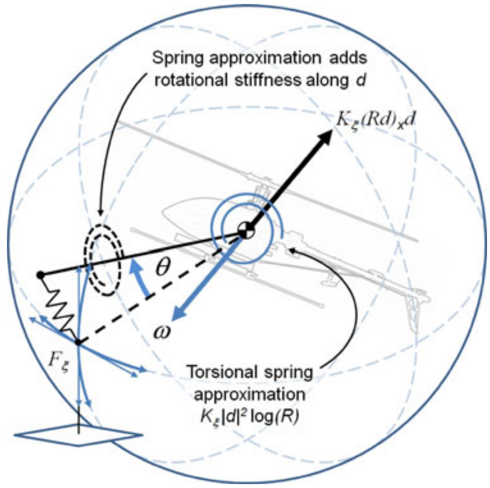

Fig. 7. Translational spring rotational approximation.

angular control will be resisted by the passive rotational elasticity. The proportional control term must dominate, such that eigenvalues of the total effective proportional stiffness matrix $K_{R_\Sigma} = k_{Rp}I + k_R I + K_\xi ||\mathbf{d}||^2$ also satisfy (22) for some range of $||R(0)||$ and $||\boldsymbol{\Omega}(0)||$.

Given the constant disturbance moment induced by the translational spring force, the system will not reach equilibrium around $R = R^d$. The equilibrium point for this system will instead occur where the combined proportional torques balance the bias torque:

$$0 = -K_{R_\Sigma}\psi - \mathbf{d}_\times K_\xi \boldsymbol{\xi}. \tag{28}$$

The biased steady-state orientation of the system can be computed through the rotation matrix exponential map:

$$R_\mathrm{B} = \exp\{(-K_{R_\Sigma}^{-1}\mathbf{d}_\times K_\xi \boldsymbol{\xi})_\times\} \tag{29}$$

where the mapping $\exp : \mathfrak{so}(3) \to SO(3)$ is

$$R = I + \sin(\theta)\boldsymbol{\omega}_\times + (1-\cos(\theta)){\boldsymbol{\omega}_\times}^2. \tag{30}$$

Within the bound $|\theta| < \pi$, the elastic rotation function is convex—given an equilibrium within this limit, the derivative of the associated energy function will be negative definite. Consequently, the biased system will remain bounded around the equilibrium.

2) Translation: The translational velocity dynamics with added compliance given in (26) can be rewritten to group constant, proportional, and rotation force components. As with the rotational case, the force from angular stiffness coupling needs to be recast as a force in the inertial frame. The exponential rotation structure is approximated by $\mathbf{d}_\times\theta\boldsymbol{\omega} = (\mathbf{d} - R\mathbf{d})$, such that

$$\begin{aligned} m\dot{\mathbf{v}} = &\ (mg\mathbf{e}_z + K_\xi\mathbf{d} + k_R||\mathbf{d}||^{-2}\mathbf{d}) - K_\xi\boldsymbol{\xi} \\ &-R(T\mathbf{e}_3 + K_\xi\mathbf{d} + k_R||\mathbf{d}||^{-2}\mathbf{d}). \end{aligned} \tag{31}$$

The contributions of the combined translational compliance, $K_{\xi_\Sigma} = K_\xi + k_R||\mathbf{d}||^{-2}$, are applied equally to the gravity force and the rotor thrust force. These additional terms can be thought of as an apparent skewing of the gravity normal plane and have the effect of a positive scaling and rotation applied to the two forces

$$m\dot{\mathbf{v}} = (mg\mathbf{e}_z + K_{\xi_\Sigma}\mathbf{d}) - R(T\mathbf{e}_3 + K_{\xi_\Sigma}\mathbf{d}) - K_\xi\boldsymbol{\xi}. \tag{32}$$

This is structurally similar to the stable free air dynamics, except that any commanded control action applies a corresponding force error. In feedback, U_ξ applied to counteract this error leads to further error. For the system to be stable, control action must dominate the corresponding induced error such that cumulative error tends to zero. If $T \approx mg$, then this requires

$$\|K_{\xi_\Sigma}\mathbf{d}\| < mg. \tag{33}$$

F. Coupled Stability

As in Sections 1) and 2), each second-order subsystem of the dynamics remains bounded and locally stable under added stiffness. However, the offset bias in rotation due to $\boldsymbol{\xi}$ couples into translational dynamics by producing nonzero lateral forces.

When aircraft orientation is approximately I and the bias in rotation is small, the exponential map can be approximated by its first-order elements $R = I + \theta\boldsymbol{\omega}_\times$. The bias orientation becomes

$$R_\mathrm{B} = I + (-K_{R_\Sigma}^{-1}\mathbf{d}_\times K_\xi\boldsymbol{\xi})_\times. \tag{34}$$

Translational velocity dynamics of (31) can then be written independent of rotation, canceling constant terms, asserting $T \approx mg$, and combining $mg\mathbf{e}_z$ and $RT\mathbf{e}_3$ to implement position control:

$$\begin{aligned} m\dot{\mathbf{v}} = &\ -K_{\xi p}\boldsymbol{\xi} - K_{\xi d}\mathbf{v} - K_\xi\boldsymbol{\xi} \\ &-(-K_{R_\Sigma}^{-1}\mathbf{d}_\times K_\xi\boldsymbol{\xi})_\times(mg\mathbf{e}_3 + K_{\xi_\Sigma}\mathbf{d}). \end{aligned} \tag{35}$$

Straightforward manipulation puts this in the form of a proportional system:

$$\begin{aligned} m\dot{\mathbf{v}} = &\ -[K_{\xi p} + K_\xi + (mg\mathbf{e}_3 + K_{\xi_\Sigma}\mathbf{d})_\times(K_{R_\Sigma}^{-1}\mathbf{d}_\times K_\xi)]\boldsymbol{\xi} \\ &-K_{\xi d}\mathbf{v}. \end{aligned} \tag{36}$$

This system will be stable around equilibrium if the eigenvalues of the proportional coefficient are positive, as follows:

$$\lambda(K_{\xi p} + K_\xi + (mg\mathbf{e}_3 + K_{\xi_\Sigma}\mathbf{d})_\times(K_{R_\Sigma}^{-1}\mathbf{d}_\times K_\xi)) > 0. \tag{37}$$

For isotropic stiffness and control gains in the form $K = kI$, these can be automatically calculated symbolically in MATLAB as

$$\boldsymbol{\lambda} = \begin{pmatrix} (k_{R_\Sigma} - mgd_3 - k_{\xi_\Sigma}\mathbf{d}'\mathbf{d})(k_{\xi p} + k_\xi)/k_{R_\Sigma} \\ (k_{R_\Sigma} - mgd_3 - k_{\xi_\Sigma}\mathbf{d}'\mathbf{d})(k_{\xi p} + k_\xi)/k_{R_\Sigma} \\ k_{\xi p} + k_\xi \end{pmatrix}. \tag{38}$$

For expected small lateral stiffness and end-effector offsets, the stability condition is approximately $k_{R_\Sigma} > mgd_3$.

TABLE I
STANDARD YALE AERIAL MANIPULATOR PARAMETERS

Aircraft Parameters					
g	9.81	$\mathrm{m \cdot s^{-2}}$	J_{xx}	0.08	$\mathrm{kg \cdot m^2}$
m	3.3	kg	J_{yy}	0.19	$\mathrm{kg \cdot m^2}$
$\mathbf{h}$	$[0\ 0\ -0.2]'$	m	J_{zz}	0.19	$\mathrm{kg \cdot m^2}$
q_1	0.0039		w_0	96	$\mathrm{rad \cdot s^{-1}}$
q_2	0.0266				
Control Parameters					
k_{Rp}	1.80		$k_{\xi p}$	2	
k_{Rd}	1.57		$k_{\xi d}$	3	
Standard Gripper Position and Approximate Isotropic Stiffnesses					
$\mathbf{d}$	$[0\ 0\ 0.2]'$	m			
k_R	2.85	$\mathrm{N \cdot m \cdot rad^{-1}}$	k_ξ	26.6	$\mathrm{N \cdot m^{-1}}$

G. Simulation

Stability bounds (38) and (33) were tested by simulating a variety of end-effector stiffness and position configurations using the full dynamics of Section II-A. Base aircraft, control, and stiffness parameters used are those of the Yale Aerial Manipulator and its gripper (see Table I). Each simulation starts with $R(0) = I$, $\mathbf{\Omega}(0) = 0$, $\boldsymbol{\xi}(0) = [0\ 0{-}0.5]'$ m, and initial velocity $\mathbf{v}(0) = [0.5\ 0\ 0]'\ \mathrm{m \cdot s^{-1}}$. The simulator is available online.[5]

We present six illustrative simulations: the standard configuration and five gripper and stiffness variations thereof, which test the stiffness ratio, contact height, and contact length bounds:

1) The standard configuration, as built.[6]
2) Standard placement, no rotational gripper stiffness.
3) Standard stiffness, gripper 0.2 m above the CoG.
4) Standard stiffness, gripper 1 m below the CoG.
5) Standard stiffness, gripper 1 m ahead of the CoG.
6) Standard stiffness, gripper 1 m right of the CoG.

Time evolution plots of simulated aircraft pose states are given in Appendix D (see Figs. 1–6); the ground end of the contact spring is fixed. The control reference position is the starting position $\boldsymbol{\xi}(0)$.

As expected from previous experiments with the Yale Aerial Manipulator, simulation 1 shows the aircraft is stable in gripping contact. However, simulation 2 indicates that the same system with no rotation stiffness will slowly topple, crashing into the ground at $t = 5.88$ s; this is homologous to dynamic rollover behavior. In contrast, when the gripper is placed at the same distance above the center of gravity, the system oscillates unstably (terminating at $t = 4.25$ s). As the contact point is set far from the CoG, system stability diminishes: In simulation 4, rotational stiffness is insufficient to stabilize the aircraft, crashing at $t = 3.61$ s. Notably, simulations 5 and 6 are not pathological. In simulation 5, the aircraft is excited along the line of the contact probe, producing no cross-coupled disturbance except for small coupling due to flapping, and the system oscillates with stable decay. Simulation 6 shows the aircraft pivot and yaw about its contact point; as the disturbance trajectory is orthogonal to gravity, the otherwise unstable motion is arrested by yaw control.

[5]http://robotics.itee.uq.edu.au/ pep/doc/YAM_simulator.zip
[6]Gripper placement and stiffness parameters as per Table II.

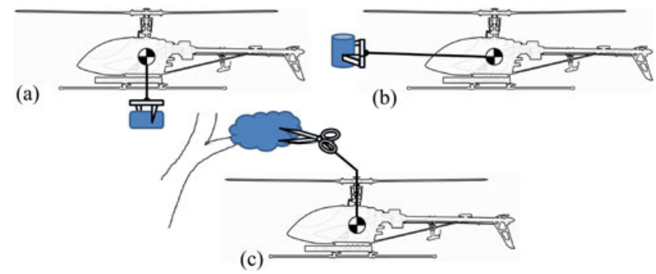

Fig. 8. Possible contact configurations: (a) $d_3 > 0$, (b) $d_3 \approx 0$, (c) $d_3 < 0$.

H. Assumptions, Implications, and Limitations

While the dynamic model given in Section II and used in the simulations is comprehensive, the analysis is by no means a complete exploration of the problem. It considers only the most common flight condition of level hovering flight, and many assumptions are made:

1) time-scale separation of dynamical subsystems;
2) approximately level flight;
3) high-gain attitude control, low-gain position control;
4) no integral action in the flight control;
5) pure rotor torques (zero lateral rotor force contribution);
6) spring force contact approximations;
7) no environment compliance, slipping, or chattering.

The key observation is that aggressive proportional attitude gain is paramount for highly robust stable contact. Rotational end-effector compliance augments the proportional attitude control without influencing free air performance, and therefore, this stiffness should be made large. However, inadvertent contacts are likely to be essentially point contacts, and therefore, a conservative design will rely only on flight control gain.

1) Implications for Manipulator Design: We identify three major classes of aerial manipulator by the vertical offset of the end-effector d_3: contact point substantially below the CoG, substantially above the CoG (e.g., connected through the rotor mast or through the body of a quadrotor), or approximately level with the CoG (see Fig. 8). Given an aircraft and flight-controller with fixed parameters, d_3 should be minimized to reduce the magnitude of torques being transmitted to the attitude dynamics. Free air stability of laden helicopters with dynamics loads also benefits from small displacements from the CoG [17]. However, this understanding assumes the rotational dynamics of the aircraft in contact reach equilibrium much faster than translational dynamics. Although the planar analysis also showed improved stability performance with shorter end-effector link lengths [16], a resulting increase in coupled-system natural frequency could be deleterious to stability of nontimescale separated systems.

Notably, (38) implies that the system should be inherently stable for some negative values of d_3; however, (33) permits only a small range of these. The full simulation shows that coupling effects that are benign and ignored in the positive configuration are pathological when the contact point is above the center of mass. In particular, horizontal rotor forces, position control, and pitch-translation coupling in the spring destabilize the system, and higher attitude gain serves to exacerbate the effect. Given

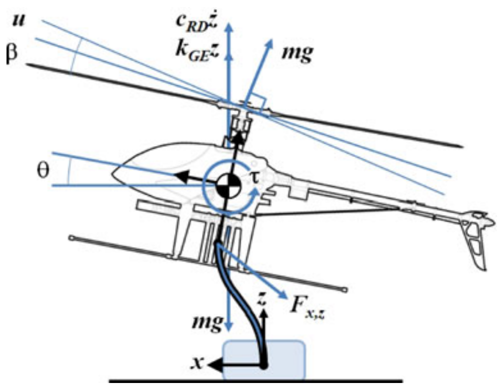

Fig. 9. Helicopter dynamic model with elastic linkage.

the rotor-over-body construction of most helicopters, d_3 is likely to be positive or only slightly negative, as an end-effector cannot easily penetrate the disc of the rotor.

Lateral offset of the end-effector tends to induce slow yaw divergence, but as yaw control can be very high gain in helicopters,[7] lateral offset is not considered pathological.

III. Planar Model and Stability

Of the assumptions identified in Section II-H, the rotor flapping effects and coupled rotation-translation modes are the most important to real-world rotorcraft. To show that these effects are not pathological, and to better represent the operation of commercial PID controllers, we must extend the analysis to include them. However, as previously discussed, the complete dynamics of Section II are difficult to develop into an explicit solution. Furthermore, integral control action on SO(3) is difficult to define, and most commercial flight control systems are SISO control laws. Thus, we consider the complete pitch-translation mechanics as SISO systems in isolation so that analytical bounds on end-effector stiffness can be found.

In particular, we aim to determine stability regions for the standard configuration described in Section II-G. In this case, where the end-effector link is short and directly beneath the center of mass, the aircraft will be operating exclusively around the equilibrium over the tether point, in low-velocity flight. In this section, we extend the analysis to include rotor flapping, ground effect, and rotor inflow damping, but exclude the effect of position control.

A. Planar Helicopter Flight Model

Helicopters lateral and longitudinal dynamics are largely decoupled around hover, and approximately linear. We consider longitudinal dynamics in particular, but the analysis is equally applicable to lateral flight near hover. We also consider ground effect force and rotor inflow damping.

The rigid-body dynamics of the linearized planar helicopter in hover are[8]

$$m\ddot{x} = -mg\beta - mg\theta - mgu + F_x \tag{39}$$

$$m\ddot{z} = -F_{\mathrm{RD}} - F_{\mathrm{GE}} + F_z \tag{40}$$

$$\mathrm{I}\ddot{\theta} = mgh\beta + mghu + \tau \tag{41}$$

where m is the mass of the helicopter; I is the pitch rotational inertia of the helicopter; g is the acceleration due to gravity; x, z, and θ are the longitudinal, vertical, and angular positions of the center of mass, respectively; h is the rotor height above the center of mass; β is the first harmonic longitudinal rotor flapping angle; u is the cyclic pitch control input; F_{RD} is rotor inflow damping; F_{GE} is effective ground effect force; and F_x, F_z, and τ are the longitudinal force, vertical force, and pitch moment applied by the linkage, respectively (see Fig. 9).

When operating in ground effect the wake of the rotor pushes against the surface underneath it, creating a cushion of air that resists the helicopter's descent. The ratio of thrust in ground effect, T_{GE}, to thrust in free air, T_{FA}, is [10]

$$\frac{T_{\mathrm{GE}}}{T_{\mathrm{FA}}} = \frac{16z^2}{16z^2 - r^2} \tag{42}$$

where r is the rotor radius.

The increase in thrust close to ground is treated as force applied as a function of distance away from the trimmed equilibrium hover altitude, z_0 (taken as $z = 0$). This can be treated like a spring force $F_{\mathrm{GE}} = k_{\mathrm{GE}} z$, where

$$k_{\mathrm{GE}} = \left[\frac{32z_0}{r^2 - 16z_0^2} + \frac{512z_0^3}{(r^2 - 16z_0^2)^2}\right]. \tag{43}$$

Vertical motion of a rotor through its own induced flow changes the local flow angle of attack at blades, which alters the amount of lift produced. This change in thrust is in the opposing direction of motion, producing vertical damping. The damping force produced is $F_{\mathrm{RD}} = c_{\mathrm{RD}}\dot{z}$ [9], where

$$c_{\mathrm{RD}} = \left[\frac{a}{4}\frac{\sigma}{\omega r}\right]\rho\pi r^2(\omega r)^2. \tag{44}$$

B. Flight Control and Free Air Stability

Helicopter pitch and longitudinal motion are strongly interdependent, but vertical motion is effectively decoupled from these around hover. Solving the longitudinal translation-pitch equations together produces a SISO transfer function between the cyclic control input and the pitch angle in free flight:

$$H = \frac{mghG - m^2g^2hq_1}{\mathrm{I}s^2G + mghq_2Gs - m^2g^2hq_1(q_2s - 1)} \tag{45}$$

where $G = ms + mgq_1$.

For flight stabilization with PID, the controller transfer function has the form

$$C = k\left(1 + \frac{k_i}{s} + k_d s\right) \tag{46}$$

[7]Quadrotors, which have limited yaw control authority, are expected to be especially susceptible to lateral offset instability, however.

[8]Rotor thrust is taken as constant, exactly canceling helicopter weight and, therefore, is not included in the vertical dynamics.

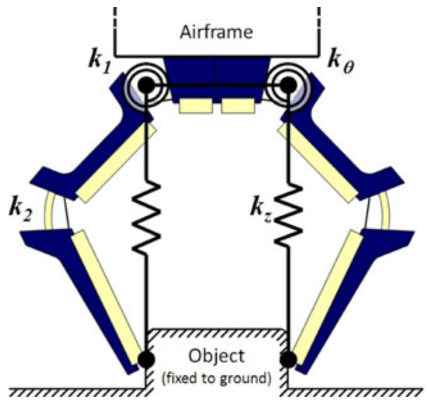

Fig. 10. Bogie suspension gripper model.

where k is the control gain, and k_i and k_d are the integral and differential control parameters, respectively.

The stability of the controlled system can be assessed by examining the characteristic polynomial of the closed-loop transfer function. Substituting (45) and (46),

$$s^3+\left(\frac{mgh}{\mathrm{I}}(q_2+kk_d)+q_1g\right)s^2+k\frac{mgh}{\mathrm{I}}s+\frac{mgh}{\mathrm{I}}(kk_i+q_1). \tag{47}$$

As the controlled helicopter is stable in free air, this polynomial is known to be stable, and its coefficients satisfy the Routh–Hurwitz criterion, which we will use for stability analysis. To be stable, a characteristic polynomial must have all positive coefficients, and that leading entries in the Routh–Hurwitz array derived from those coefficients must be positive [11]. It can be shown that for free air stability

$$-\mathrm{I}q_1g-\mathrm{I}kk_i+\mathrm{I}q_1gk+mghk(q_2+kk_d)>0 \tag{48}$$

which is later used in factorizing polynomial elements for the tethered case (see Appendix C).

C. Contact Model

As seen from Section II-C, a planar contact model can be implemented as a combination of translational stiffness in longitudinal and vertical motions and rotational stiffness in pitch. In our specific application of grasping from a helicopter, the elastic linkage being investigated is a compliant gripper mechanism. The gripper consists of four fingers, each with two links and two elastic flexures at the proximal and distal joints, with stiffnesses k_1 and k_2, respectively. In the planar case, the gripper is treated as two axis-symmetric nonslip contact points representing opposing pairs of fingers (see Fig. 10).[9] The rotor thrust balances the weight of the helicopter; the grasped object is considered rigidly fixed to the ground.

Each finger can be modeled as a prismatic spring with a torsional spring at the proximal joint, where the equivalent spring

[9]The lateral view of the gripper is shown here for clarity—the same model can be used both for small lateral and longitudinal motions of the gripper, where k_1 is the out-of-plane stiffness of the proximal flexural element.

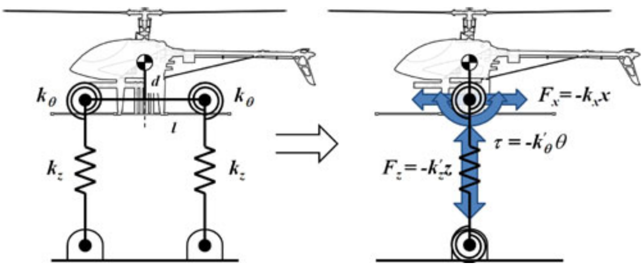

Fig. 11. Bogie suspension single link approximation.

stiffnesses k_z and k_θ are given by

$$k_\theta = k_1 \tag{49}$$

$$k_z = \frac{k_1k_2}{k_1+k_2}\frac{1}{r^2} \tag{50}$$

where k_θ is the torsional spring stiffness, k_z is the prismatic spring stiffness, and $l = l_f \sin\frac{\pi}{4}$ is the lever arm from the gripper centre axis and proximal joint, assuming that the proximal and distal links are of equal length l_f.

Around equilibrium, the elastic forces and torques applied due to x, z, and θ motion are approximately decoupled, and the planar bogie suspension configuration can be approximated as a single elastic linkage with tension springs at both pin joints (see Fig. 11). The springs of the equivalent single linkage, k'_z, k'_θ, and k_x, are computed by

$$k'_z = 2k_z \tag{51}$$

$$k'_\theta = 2k_zl^2+2k_\theta \tag{52}$$

$$k_x = 2k_\theta. \tag{53}$$

Note that l is the distance between the tether point and the bogie pin joint—corresponding to the proximal joint of the gripper.

This model conforms to the decoupled anisotropic stiffness model of Fig. 17 and is valid for the case where the helicopter thrust exactly equals its own weight; lateral stiffness induced by vertical thrust is zero in this case. However, as the helicopter begins to apply thrust to ascend, the vertical force applied to the end of the linkage will induce a lateral kinematic stiffness in addition to the elastic stiffness of the linkage:

$$F_x = -\left(k_x+\frac{\delta T}{d}\right)x \tag{54}$$

where δT is the additional applied thrust, up to the weight of the carried object m_0g. The combined stiffness term is denoted as k'_x. For large carried masses, this stiffness can be greater than that of the linkage.

When the thrust applied exceeds the combined weight of the helicopter, the object leaves the ground and the craft transitions to suspended load behavior, the mechanics of which have been explored in detail elsewhere [12], [13]. This linkage model can also be extended to other related constraint scenarios such as motion of flexible landing skids on landing or adapted to novel cases such as compliant connections to objects suspended by swarms of UAVs.

D. Vertical Stability

Motion in the z-direction is independent of longitudinal and pitch motion and is not directly regulated by the flight controller—it must be intrinsically stable to reject disturbances. Using the standard linear spring–displacement model, the equation of motion of the system in vertical motion becomes

$$m\ddot{z} = -c_{\mathrm{RD}}\,\dot{z} - (k_{\mathrm{GE}} + k'_z)z. \tag{55}$$

The Laplace transform yields the characteristic polynomial

$$s^2 + \frac{c_{\mathrm{RD}}}{m}s + \frac{k_{\mathrm{GE}} + k'_z}{m}. \tag{56}$$

By inspection, this system is stable for physical values.

E. Pitch-Translation Stability

The horizontal dynamics of the system can be analyzed in the same way as the vertical dynamics. Note that the longitudinal translation of the system is coupled back into the pitch dynamics through the moment produced around linkage offset d directly below the center of mass (equivalent to $\mathbf{d} = [0\ 0\ d]$). The dynamic equation of the tethered plant is

$$H' = \frac{mghG - mgq_1(mghs - dk'_x)}{\mathrm{I}Gs^2 + mghq_2Gs - mgq_1(mghs - dk'_x)(q_2s - 1) + Gk'_\theta} \tag{57}$$

where

$$G = ms^2 + mgq_1s + k'_x \tag{58}$$

gives the poles of the translational dynamics.

Using the control law given in (46), the characteristic equation of the closed-loop system is a fifth-order polynomial (see Appendix B), with three variable parameters: effective stiffnesses k'_θ and k'_x, and the gripper distance below the center of gravity, d. As the flight controller is considered fixed, suitable bounds must be found on these parameters to guarantee stability.

Not all of the polynomial coefficients are unconditionally positive—the fourth coefficient, a_4, is only guaranteed positive for all k'_θ and k'_x when $k(h + d) > d$. As d is a physical parameter of the helicopter and is not easily changed, it may be considered effectively fixed. Asserting that k is great than unity, and thus, $a_4 > 0$ is satisfied, only variation in linkage stiffness will be considered.

The four leading entries of the Routh–Hurwitz array, i.e., b_1, c_1, d_1, and e_1, must all be positive for the system to be stable. With the exception of c_2 and e_1, the equations for the array elements are long and these are given in Appendix C. To understand what regions of stability exist, the value of each entry may be plotted as a function of k'_θ and k'_x, superimposed on a single graph showing the region in which all parameters are positive (see Fig. 12).

Explicit bounds may be found by analyzing the equations for b_1, c_1, and d_1. Factorization of these entries is lengthy, but yields the key constraint for stability, given arbitrarily large values of k'_θ and k'_x as

$$hmk'_\theta - d\mathrm{I}k'_x > 0. \tag{59}$$

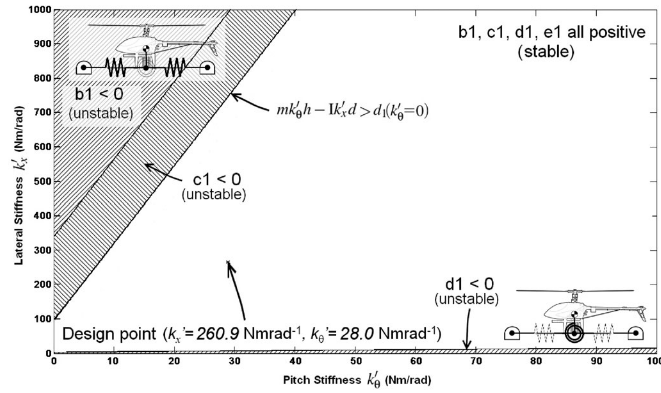

Fig. 12. Stability bounds for linkage stiffnesses.

TABLE II
AIRCRAFT, CONTROL, AND GRIPPER PARAMETERS

			Aircraft Parameters		
g	9.81	$\mathrm{m \cdot s^{-2}}$	ρ	1.184	$\mathrm{kg \cdot m^{-3}}$
m	4.3	kg	I	0.1909	$\mathrm{kg \cdot m^2}$
ω	96	$\mathrm{rad \cdot s^{-1}}$	R	0.74	m
h	0.2	m	a	5.5	$\mathrm{rad^{-1}}$
q_1	0.0039		q_2	0.0266	
			Control Parameters		
k	1.8		k_d	1.57	
k_i	1				
			Gripper Parameters		
k'_x	260.9 $\mathrm{N \cdot m \cdot rad^{-1}}$	k'_θ	28.0	$\mathrm{N \cdot m \cdot rad^{-1}}$	
d	0.2	m			

This inequality is derived from c_1 but is also required for d_1. There is a region of stability under the intercept at $k'_\theta = 0$. This margin can be calculated explicitly by determining $d_1 = 0$ for $k'_x = 0$, which has the solution given in the appendix. A second inequality constrains very low angular stiffness in d_1, but real mechanisms will typically satisfy this minimal bound.

Intuitively, the stable and unstable regimes can be understood at extrema as either a helicopter fixed level but free to translate ($k'_\theta = \infty, k'_x \approx 0$), or a helicopter pinned to a rigid fixture but free to rotate ($k'_\theta = 0, k'_x = \infty$)—analogous to an inverted pendulum.

F. Proof-of-Concept System Parameters and Stability

The stability of the proof-of-concept system previously described can be determined using the helicopter, controller, and gripper parameters given in Table II. Gripper stiffness values were determined empirically. By applying (48), it can be readily verified that the specified PID parameters stabilize the helicopter in free flight.

Computing the tethered stability conditions, it is seen that the gripper offset requirement, $k(h + d) - d$, is satisfied, but the rotational and lateral stiffnesses k'_θ and k'_x produced by the proximal and distal joints do not alone satisfy the slope requirement of (59). It is, therefore, necessary to compute the intercept at $k'_\theta = 0$ to ascertain if the parameters are in the stable region. Using (74) and (59), the stability bound intercept is

$98.3\ \mathrm{N \cdot m \cdot rad^{-1}}$, and the slope is 48.48, placing the system well within stable operating conditions. This provides good confidence that the helicopter–gripper system can be hovered in a grasping configuration without inducing instability.

G. Assumptions, Implications, and Limitations

This analysis is valid for planar mechanics of a helicopter near hover (either pitch or roll motion); with rotor flapping effect, ground effect, and rotor inflow damping; and an end-effector located directly beneath the center of mass, using anisotropic stiffnesses. It is assumed that the aircraft is constrained not to move out of the plane; longitudinal–lateral rotor cross-coupling effects are ignored. This analysis does not consider the effect of high-speed flight, or ground vortex roll-up due to fast translation near ground. This derivation also specifically takes into account cross-coupling effects that earlier derivations omitted [16].

Unlike the 6-DOF system, this analysis considers the simultaneous coupled mechanics of the rotation and translation systems. The stability bounds derived in Section III-E are compatible with the findings of Section II-H, showing a linear bound from a given ratio of translational and rotational stiffnesses. Of particular interest is the role played by rotor height above the center of gravity — a parameter not considered by "flying brick" models — and the duality between vertical gripper displacement and mass-inertial ratio. This indicates that the two competing influences of the rotation–translation system can be traded off against each other. Potentially, this could allow for the creation of task-specific UAVs where the mechanical parameters of the aircraft are optimized for the aerial manipulation task, indicated in Fig. 8.

IV. Experiments

In this section, we describe experimental tests following from the preceding analysis. In particular, we had three objectives. First, we seek to show that the "standard configuration" of the test platform when hovering coupled to ground is stable as predicted. Second, we seek to show that a configuration that is near the unstable gripper placement bounds exhibits marginal stability. Finally, we seek to show the stability of the aircraft grasping an object during transition to free flight.

A. Dynamic Response of Coupled-Hover Configurations

Object interaction experiments with a gripper near the helicopter center of mass necessarily involves risky flight close to the ground, where little response time is available to recover the aircraft in an emergency. A test-rig was designed to emulate the isotropic stiffness of the compliant manipulator described in Section III-C, while keeping the test vehicle far above the ground. As discussed in Section II-H, extending the length of the gripper offset decreases the stability of the system. We chose to test a stable configuration near the stability boundary as a "worst-case" end-effector design.

The apparatus uses a network of equal springs acting around a center framework to produce an accurately known force–torque couple at the center of compliance (see Fig. 13). Low-friction bearings around the spring element mountings permit only the linear force of the springs to be transmitted to the framework. A shaft protrudes from the framework, terminating in a ferromagnetic fixture that allows a helicopter to couple to the structure. A T-Rex 600 helicopter fitted with a Helicommand Profi flight stabilizer was equipped with a mating electromagnet couple and docking cone.

Fig. 13. Helicopter test platform coupled to sprung compliance framework.

The spring stiffnesses and offsets were chosen to make the net translation and rotational stiffnesses equal to that of the gripper module: $260.9\ \mathrm{N \cdot m^{-1}}$ and $28.0\ \mathrm{N \cdot m \cdot rad^{-1}}$. The distance between the helicopter center of mass and the sprung framework's center of compliance was set to 1 m — at the edge of the stability bound. Stability of this system indicates that the more conservative gripper system will also be stable.

The helicopter was held in hover and allowed to come to rest coupled to the magnetic fixture. Once the system had settled, the framework was perturbed by applying a force at the bottom spring mounting by a lightweight string tugged to a displacement of 125 mm, and then released. This caused the aircraft to be displaced in both angle and position, and the aircraft was allowed to respond and settle — the resulting motion of the aircraft was seen to be stable. Two successive perturbations of the system and the stable recovery of the aircraft are shown in Fig. 14.

B. Hovering Coupled to a Fixed Object

To explore the actual stability of the aircraft in coupled hovering under PID control, we used the test aircraft fitted with the gripper module to grasp a wood block attached to the ground (see Fig. 15). The aircraft was flown into position under control of a human safety pilot with landing gear retracted and then switched to autonomous PID hover as the gripper was closed.

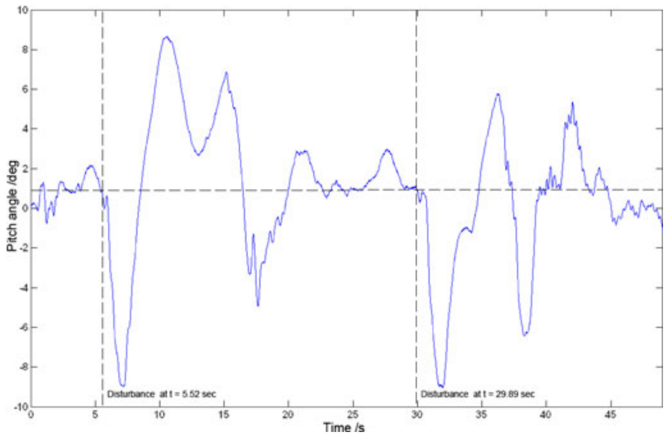

Fig. 14. Pitch response of coupled aircraft to disturbance.

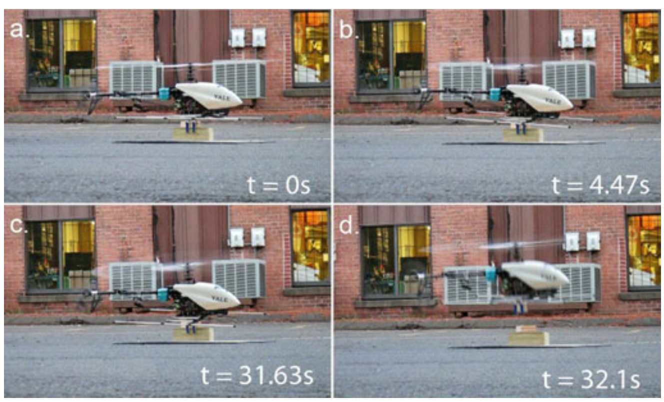

Fig. 15. Coupled hovering, grasping a block fixed to ground.

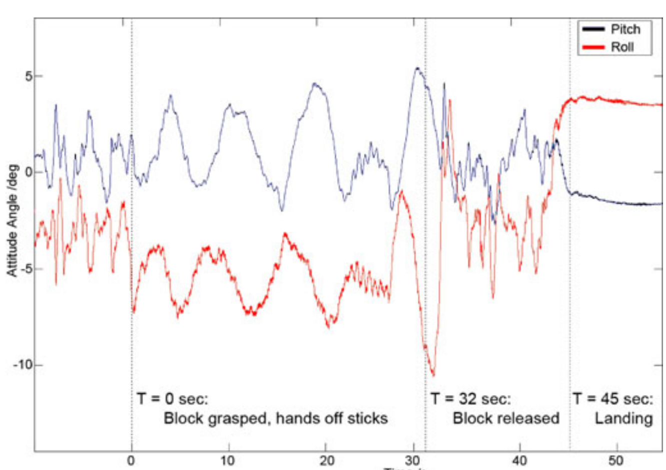

Fig. 16. Coupled hovering pitch and roll angles.

For the duration of the experiment, the hover thrust was maintained, and the pilot did not issue commands to the vehicle.

After achieving a grasp, the vehicle remained stable; the aircraft gripper was released after 32 s [see Figs. 15(d) and 16]. The slow oscillation of the aircraft during contact hover is thought to be due to wind eddy currents in the outdoor test facility. The experiment was repeated, with the aircraft hovering in contact for 26 s. The aircraft did not touch the ground during either trial.

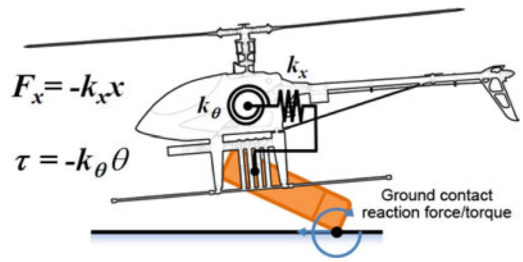

Fig. 17. Transitional contact force coupling model.

C. Transition to Free Flight

Once grasped, retrieving the object requires the helicopter to apply increased thrust to balance the weight of the payload and transition to free flight. As the surface normal force reduces, the lateral force produced by object contact friction will decrease—eventually the object slips, resulting in much reduced lateral stiffness. Similarly, the ground torque reaction decreases, devolving to single-point contact with only kinematic angular stiffness, until the payload begins to lift clear (see Fig. 17).

Continued stability in partial contact depends on the object geometry and contact properties. A long flat object on ice will slide freely but hold the helicopter level, while a sticky rubber sphere on tarmac will act like a pin joint, potentially causing the helicopter to pivot into the ground.

In practice, transient contact conditions are difficult to maintain, due to the sensitivity of the helicopter to disturbances—as the applied thrust exceeds the net mass of the vehicle, the aircraft quickly loses contact with the ground. However, when grasping round objects, tractive objects with short base lengths, this transition should be made quickly so that instantaneous unstable conditions do not persist long enough to pose a danger to the aircraft.

D. Object Retrieval While Hovering

Complete operation of the Yale Aerial Manipulator grasping subsystem was demonstrated by gripping and retrieving a variety of objects while hovering under PID control. Similar to the coupled grasping experiment, the helicopter was positioned over the target, switched to autonomous hover mode, and the gripper closed. Once the grasp was secure, rotor collective was increased until the object lifted clear the ground (see Fig. 18).

We successfully retrieved unstructured object 18 times; no trials exhibited instability or caused the helicopter to touch the ground while grasping. Objects grasped include a wood block (700 g, 265 mm), PVC cylinder (900 g, 390 mm), softball (160 g, 89 mm), and a weighted tool case (1.45 kg, 335 mm; see Fig. 19). The block grasping and ground-coupled experiments described above are documented in the video attached to this paper.

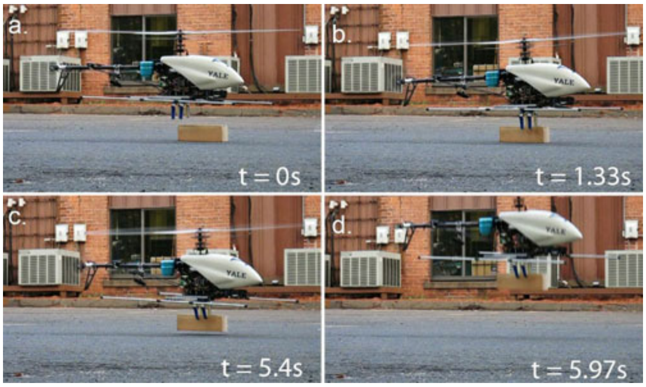

Fig. 18. Grasp and retrieval of a block while in hover.

Fig. 19. Yale aerial manipulator retrieving a 1.5-kg tool case.

V. Conclusion

This paper is a preliminary effort at understanding the problem of PD-stabilized hovering aircraft—and helicopters in particular—manipulating objects, focusing on the most important configuration of compliant contact at low velocities in level hover. This study presented a 6-DOF helicopter dynamic model with elastic contact constraints and expanded it with a complete aerodynamics rotor model in the planar case, including rotor flapping mechanics, inflow damping, and ground effect. We described a PD/PID control structure for rotation and position control, assuming time-scale separation in the 6-DOF system.

Using a Lyapunov stability metric and Routh–Hurwitz criterion analysis, we determined bounds for each system on contact stiffness parameters that ensure the stability of the aircraft. Simulation of the full dynamic model confirms the stability transitions predicted by the analytical model. The stability configurations of each analytic system are in agreement.

By applying these constraints to the known parameters of a proof-of-concept aircraft gripper and controller, it was shown that the test configuration is well within the stable region of the constraints. A sprung dynamics testbed was used to verify stability of the elastically coupled aircraft system near the stability transition; the aircraft rejected applied disturbance inputs transmitted through the end-effector link. Finally, the complete system demonstrated stable coupling to an object using an elastic gripper.

The key insight for aerial manipulation is that for underslung end-effector contacts, high proportional attitude gain is essential for robust object interaction. Contact configurations substantially above the aircraft CoG produce pathological behavior, but lateral offsets do not significantly affect the stability of the system. There is a fundamental balance between the angular and translational stiffness of the end-effector contact; angular stiffness must always dominate translational stiffness.

Appendix A
Reconstruction of Rotation Matrix to Apply Desired Translational Force

The translational force acting on the vehicle is the sum of the rotor force vector and weight force. To apply a desired normalised control vector $\mathbf{U}_\xi$, the orientation of the vehicle must be set such that

$$mg\mathbf{U}_\xi = mg\mathbf{e}_z - TR\mathbf{e}_3. \tag{60}$$

The required R configuration to generate this control can be determined by constructing the matrix R^d as

$$R^d = \begin{pmatrix} \mathbf{R}_1^d & \mathbf{R}_2^d & \mathbf{R}_3^d \end{pmatrix} \tag{61}$$

which orients the gravity-thrust vector sum in the desired direction of motion. This is a three-step process.

First, choose vector $\mathbf{R}_3^d$ to apply the desired lateral and longitudinal force A

$$\mathbf{R}_3^d = \begin{pmatrix} -\mathbf{e}_x \cdot \mathbf{U}_\xi \\ \mathbf{e}_y \cdot \mathbf{U}_\xi \\ (1 - \mathbf{U}_\xi' P \mathbf{U}_\xi)^{\frac{1}{2}} \end{pmatrix} \tag{62}$$

using orthogonal projection matrix $P = (\mathbf{e}_1\ \mathbf{e}_2\ 0)$, such that $||\mathbf{R}_3^d|| = 1$.

Second, choose $\mathbf{R}_1^d$ such that $||\mathbf{R}_1^d|| = 1$ and $\mathbf{R}_1^d \cdot \mathbf{e}_y = 0$—this maintains a desired yaw heading of zero. Set $\mathbf{R}_2^d = \mathbf{R}_3^d \times \mathbf{R}_1^d$ such that the SO(3) group structure of R^d is maintained. This structure is resolvable provided $||\mathbf{U}_\xi P \mathbf{U}_\xi'|| < 1$.

Finally, we can determine the corresponding thrust magnitude control required to maintain altitude

$$\delta u_4 = \alpha_M^{-1} mg(\mathbf{e}_z \cdot (\mathbf{U}_\xi - \mathbf{e}_z) + R_{33}^d) \tag{63}$$

applying the required $\mathbf{e}_z$ force component.

Appendix B
Planar Coupled-Dynamics Characteristic Polynomial

Using the control law given in (46), the characteristic equation of the closed-loop system is the fifth-order polynomial:

$$s^5 + a_1 s^4 + a_2 s^3 + a_3 s^2 + a_4 s + a_5 \tag{64}$$

where

$$a_1 = ((q_2 + kk_d)m^2gh + Imgq_1)/(\mathbf{I}m) \tag{65}$$

$$a_2 = (Ik_x' + km^2gh + mk_\theta')/(\mathbf{I}m) \tag{66}$$

$$\begin{aligned} a_3 = {} & ((q_2 + kk_d)mg(h+d)k_x' + kk_i m^2 gh + (mg)^2 hq_1 \\ & + mgq_1 k_\theta' + mghq_1(k_\theta'/d))/(\mathbf{I}m) \end{aligned} \tag{67}$$

$$a_4 = (mg(k(h+d)-d)k'_x)/(\mathbf{I}m) \tag{68}$$
$$a_5 = (kk_i mg(h+d)k'_x)/(\mathbf{I}m). \tag{69}$$

APPENDIX C
STABILITY BOUND INTERCEPT

The vertical axis intercept of the shared c_1—d_1 stability bound was found by solving the c_1 stability condition for the roots of k'_x, given $k'_\theta = 0$. In c_1, this solution includes a quadratic in k'_x, yielding the two bounds observed:

$$0 = \alpha_1 k'^2_x + \alpha_2 k'_x + \alpha_3 \tag{70}$$

where

$$\alpha_1 = \mathbf{I}m^2(q_2 + kk_d)g(h+d)(\mathbf{I}q_1 g - m(q_2 + kk_d)gd) \tag{71}$$

$$\begin{aligned}\alpha_2 = {} & (m^2(q_2 + kk_d)gh + \mathbf{I}mq_1 g)((kk_i m^2 gh + m^2 ghq_1 g\mathbf{I}) \\ & + ((q_2 + kk_d)gm(h+d)(km^2 gh))) \\ & - 2(kk_i m^2 gh + m^2 ghq_1 g)((q_2 + kk_d)gm(h+d))\mathbf{I}m \\ & + (m^2(q_2 + kk_d)gh + \mathbf{I}mq_1 g)kk_i g(h+d)\mathbf{I}m^2 \\ & - (m^2(q_2 + kk_d)gh + \mathbf{I}mq_1 g)^2 g(k(h+d)-d)m\end{aligned} \tag{72}$$

$$\begin{aligned}\alpha_3 = {} & m^5 g^2 h^2 (kk_i + q_1 g) * \\ & ((q_2 + kk_d)mghk + \mathbf{I}q_1 gk - \mathbf{I}kk_i - \mathbf{I}q_1 g)\end{aligned} \tag{73}$$

with the lower stability bound given by

$$k'_{x0} = \frac{-\alpha_2 - (\alpha_2^2 - 4\alpha_1\alpha_3)^{\frac{1}{2}}}{2\alpha_1}. \tag{74}$$

APPENDIX D
SIX-DEGREE-OF-FREEDOM SIMULATION DYNAMIC RESPONSES

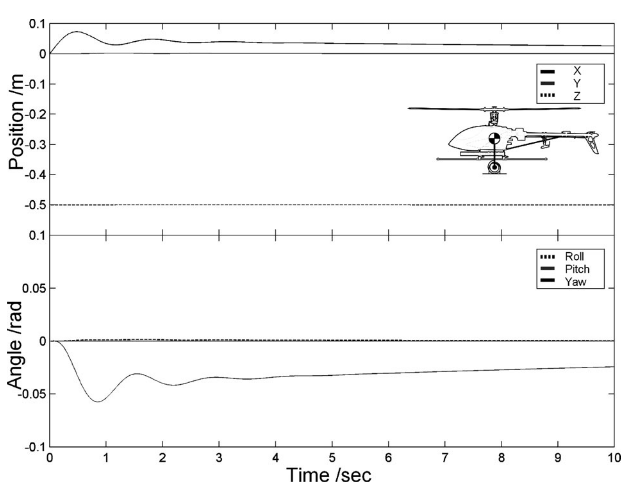

Fig. 20. Simulation 1—Standard gripper configuration. $d = [000.2]'$ m, $k_\xi = 260.9$ N $\cdot$ m^{-1}, $k_R = 28.0$ Nm $\cdot$ rad^{-1}.

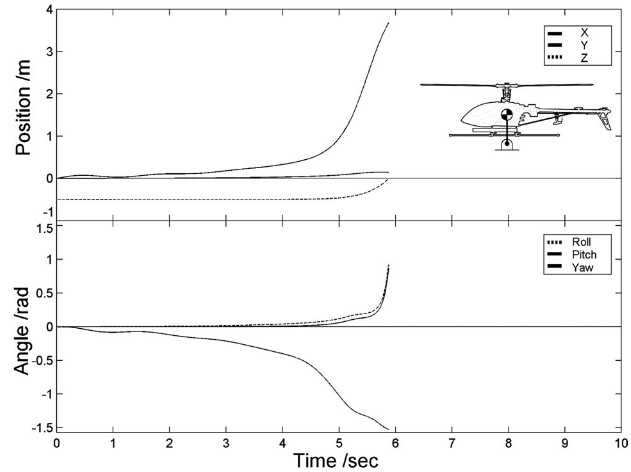

Fig. 21. Simulation 2—Zero rotational stiffness. $d = [000.2]'$ m, $k_\xi = 260.9$ N $\cdot$ m^{-1}, $k_R = 0$ Nm $\cdot$ rad^{-1}.

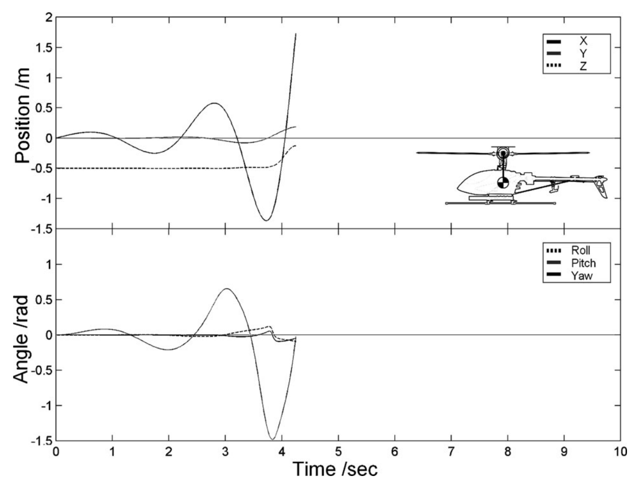

Fig. 22. Simulation 3—Inverted contact point. $d = [00-0.2]'$ m, $k_\xi = 260.9$ N $\cdot$ m^{-1}, $k_R = 28.0$ Nm $\cdot$ rad^{-1}.

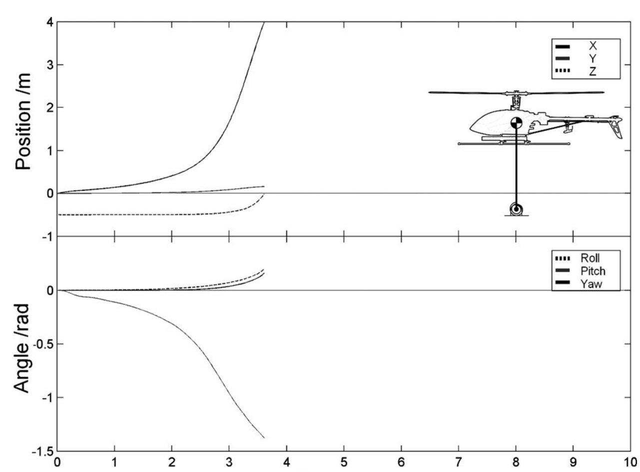

Fig. 23. Simulation 4—Extended vertical contact probe. $d = [001]'$ m, $k_\xi = 260.9$ N $\cdot$ m^{-1}, $k_R = 28.0$ Nm $\cdot$ rad^{-1}.

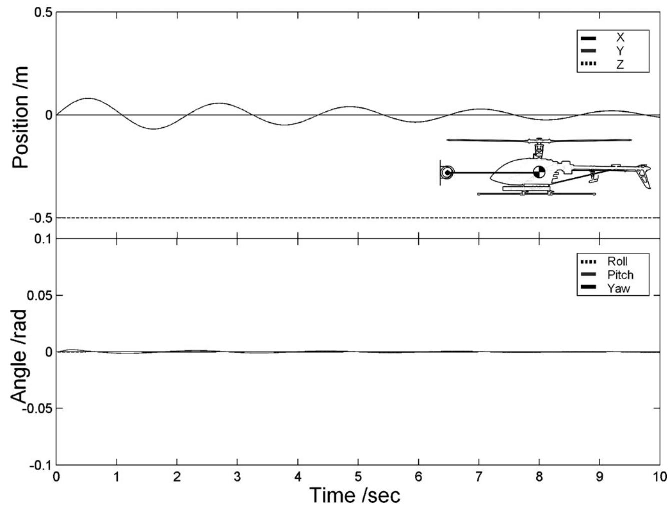

Fig. 24. Simulation 5—Extended longitudinal contact probe. $d = [100]'$ m, $k_\xi = 260.9$ N $\cdot$ m^{-1}, $k_R = 28.0$ Nm $\cdot$ rad^{-1}.

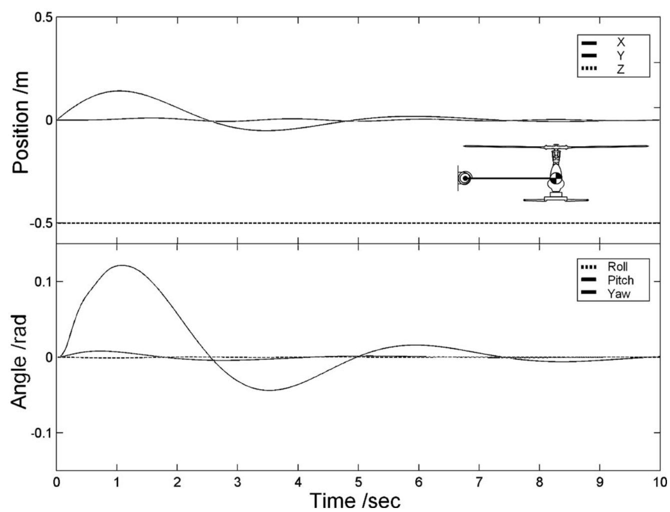

Fig. 25. Simulation 6—Extended lateral contact probe. $d = [010]'$ m, $k_\xi = 260.9$ N $\cdot$ m^{-1}, $k_R = 28.0$ Nm $\cdot$ rad^{-1}.

Acknowledgment

The authors would like to thank J. Swensen and L. Ohdner for their helpful discussion related to this work.

References

[1] L. Gentili, R. Naldi, and L. Marconi, "Modeling and control of VTOL UAVs interacting with the environment," in *Proc.IEEE Conf. Decision Control*, 2008, pp. 1231–1236.

[2] D. Mellinger, Q. Lindsey, M. Shomin, and V. Kumar, "Design, modelling, estimation and control for aerial grasping and manipulation," in *Proc. IEEE/RSJ Int. Conf. Intell. Robots Syst.*, 2011, pp. 2668–2673.

[3] L. Marconi, R. Naldi, and L. Gentili, "Modeling and control of a flying robot interacting with the environment," *Automatica*, vol. 47, no. 12, pp. 2571–2583, 2011.

[4] A. M. Dollar and R. Howe, "A robust compliant grasper via shape deposition manufacturing," *IEEE/ASME Trans. Mechatronics*, vol. 11, no. 2, pp. 154–161, Apr. 2006.

[5] L. Kaufman and E. Schultz, "The stability and control of tethered helicopters," *J. Am. Helicopter Soc.*, vol. 7, no. 4, pp. 41–54, 1962.

[6] G. Schmidt and R. Swik, "Automatic hover control of an unmanned tethered rotorplatform," *Automatica*, vol. 10, no. 4, pp. 393–394, 1974.

[7] S.-R. Oh, S. Agrawal, K. Pathak, H. R. Pota, and M. Garrett, "Autonomous helicopter landing on a moving platform using a tether," in *Proc. IEEE Int. Conf. Robot. Autom.*, 2005, pp. 3960–3965.

[8] S.-R. Oh, S. Agrawal, K. Pathak, H. R. Pota, and M. Garrett, "Approaches for a tether-guided landing of an autonomous helicopter," *IEEE Trans. Robot.*, vol. 22, no. 3, pp. 536–544, Jun. 2006.

[9] P. E. I. Pounds, R. Mahony, and P. Corke, "Modelling and control of a large quadrotor robot," *Control Eng. Practice*, vol. 18, no. 7, pp. 691–699, 2010.

[10] R. Prouty, *Helicopter Performance, Stability and Control*. London, U.K.: Krieger Publishing Company, 2002.

[11] G. F. Franklin, J. D. Powell, and A. Emami-Naeini, *Feedback Control of Dynamic Systems*. Reading, MA, USA: Addison Wesley, 1994.

[12] M. Bisgaard, J. Bendtsen, and A. la Cour-Harbo, "Modelling of generic slung load system," *J. Guid., Control Dyn.*, vol. 32, no. 2, pp. 573–585, 2009.

[13] M. Bernard and K. Kondak, "Generic slung load transportation system using small size helicopters," in *Proc. IEEE Int. Conf. Robot. Autom.*, 2009, pp. 3258–3264.

[14] J. M. Moore, "A system for landing an autonomous radio controlled helicopter on sloped terrain," Master's thesis, Dept. Aeronautics Astronautics, Massachusetts Inst. Technol., Cambridge, MA, USA, 1994.

[15] D. Cabecinhas, R. Naldi, L. Marconi, C. Silvestre, and R. Cunha, "Robust take-off and landing for a quadrotor vehicle," in *Proc. IEEE/RAS Int. Conf. Robot. Autom.*, 2010, pp. 1630–1635.

[16] P. E. I. Pounds and A. M. Dollar, "Hovering Stability of helicopters with elastic tethers," in *Proc. ASME Dyn. Syst. Control Conf.*, 2010.

[17] P. E. I. Pounds, D. R. Bersak, and A. M. Dollar, "Grasping from the air: Hovering capture and load stability," in *Proc. IEEE/RAS Int. Conf. Robot. Autom.*, 2011, pp. 2491–2498.

[18] P. E. I. Pounds and A. M. Dollar, "UAV Rotorcraft in Compliant Contact: Stability Analysis and Simulation," in *Proc. Int. Conf. Intell. Rob. Syst.*, 2011, pp. 2660–2667.

[19] R. Mahony, T. Hamel, and A. Dzul-López, "Hover control via Lyapunov control for an autonomous model helicopter," in *Proc. Conf. Decision Control*, 1999, pp. 3490–3495.

[20] B. Mettler, *Identification, Modeling and Characteristics of Miniature Rotorcraft*. Nowell, MA, USA: Kluwer, 2003.

[21] J. Loncčarić, "Passive realization of generalized springs," in *Proc. IEEE Int. Symp. Intell. Control*, 1991, pp. 116–121.

[22] F. Bullo and R. M. Murray, "Proportional derivative (PD) control on the Euclidean group," in *Proc. Eur. Control Conf.*, 1995, pp. 1091–1097.

Paul E. I. Pounds (M'06) received the B.E. degree in systems engineering and the Ph.D. degree from Australian National University, Canberra, Australia, and conducted 2.5 years of postdoctoral study with Yale University, New Haven, CT, USA.

He is a Lecturer in mechatronics with University of Queensland, Brisbane, Australia. His research interests include unmanned aerial vehicle flight dynamics, stability and control, aerial manipulation and disposable drones, and self-deploying sensors.

Dr. Pounds received the Australian Research Council 2013 Discovery Early Career Researcher Award.

Aaron M. Dollar (SM'13) received the B.S. degree in mechanical engineering from University of Massachusetts at Amherst, Amherst, MA, USA, and the S.M. and Ph.D. degrees in engineering sciences from Harvard University, Cambridge, MA, and conducted two years of postdoctoral research with the Massachusetts Institute of Technology Media Laboratory.

He is the John J. Lee Associate Professor of mechanical engineering and materials science with Yale University, New Haven, CT, USA. His research interests include human and robotic grasping and dexterous manipulation, mechanisms and machine design, and assistive and rehabilitation devices including upper-limb prosthetics and lower-limb orthoses.

Dr. Dollar received the 2014 NASA Early Career Faculty Award, the 2013 DARPA Young Faculty Award, the 2011 AFOSR Young Investigator Award, the 2010 Technology Review TR35 Young Innovator Award, and the 2010 NSF CAREER Award.